Effects of Various Imidazole Ligands on Heme Conformation in Endothelial Nitric Oxide Synthase†

Vladimir Berka,‡ Graham Palmer,§ Pei-Feng Chen,‡ and Ah-Lim Tsai*,‡

Division of Hematology, Department of Internal Medicine, University of Texas Medical School at Houston, Houston, Texas 77030, and Department of Biochemistry and Cell Biology, Rice University, Houston, Texas 77251

Received January 20, 1998; Revised Manuscript Received March 6, 1998

ABSTRACT: We have evaluated the influence of a series of substituted imidazoles on the heme structure of endothelial nitric oxide synthase (eNOS). Optical, MCD, and EPR spectra reveal widely differing effects on heme spin state and geometry. 1-Substituted imidazoles always yield low-spin heme complexes, but the size of the 2- and 4-substituent influences their structural effects on the heme. Methyl substituents lead to low-spin complexes while the bulky phenyl group yields high-spin complexes. The only exception to this behavior is provided by 2-aminoimidazole. Although this compound has three functional groups which can serve as an axial ligand to the heme, its binding to eNOS leads to a pure high-spin complex. This result can only be interpreted as due to a direct binding of 2-aminoimidazole to the guanidine binding subdomain of L-arginine. MCD spectra also imply that an O-ligand is present in the low-spin resting eNOS, while EPR data reveal the presence of two low-spin heme complexes in resting eNOS and its imidazole complexes. EPR also distinguishes four different high-spin forms of eNOS generated by different imidazole analogues. This series of ligands promises to be useful in probing the subtle structural difference among the active sites of three NOS isozymes and in developing selective inhibitors to these important enzymes.

There are at least three nitric oxide synthase (NOS)[1] hemoproteins responsible for the formation of nitric oxide, an important mediator in neural transmission, cytoprotection, and cardiovascular functions (*1*, *2*). These three isoforms of NOS share an overall 65−71% primary protein sequence homology (*3*, *4*). To develop selective reagents targeted to an individual isozyme, it is critical to understand the similarities and differences in the structure of the active site for each substrate. One approach to this goal is to use a series of homologous heme ligands to probe the environment of the heme axial coordination pocket. Many anionic ligands which are demonstrated to bind tightly with other ferric hemoproteins are not strong ligands for NOS heme, a cytochrome P450 type (*5*), due to the highly electronegative proximal thiolate ligand. Even the cyanide binding affinity for NOS is in the range of millimolar (*6, 7*). In contrast, neutral imidazole derivatives have been demonstrated to be among the few strong ligands for NOS isozymes (*7*−*12*). Thus, Wolff and co-workers have evaluated the effect of a series of imidazole derivatives on the enzyme activity of NOS isozymes (*9*, *10*) while Masters and her colleagues first examined the direct interaction of imidazole with NOS heme by spectral perturbation (*11*, *12*). This direct approach was later extended by us to kinetic and EPR analysis (*7*, *13*) and to optical and activity studies by the Merck group (*14*). The direct spectral perturbation approach appears to agree that imidazole derivatives compete directly with binding of L-arginine, while data from steady-state analysis of L-citrulline formation showed different modes of inhibition with L-arginine (*8*−*14*).

Thus far, the reported optical spectral perturbation of NOS heme by imidazole and its derivatives is a type II change (i.e., a red shift) due to formation of low-spin heme complexes (*11*−*14*). This might lead to the conclusion that all imidazole derivatives interact with NOS heme through direct ligation to the heme iron in formation of the low-spin complex. In this study, we used optical, EPR, and magnetic circular dichroism (MCD) to evaluate the effect on the heme structure of endothelial type NOS (eNOS) of a series of imidazole ligands with substituents at the 1-, 2-, or 4-positions. We find that both low-spin (type II) and high-spin (type I) complexes are formed with different imidazole analogues. Furthermore, it appears there are at least four different types of high-spin heme structures present in eNOS and eNOS complexes.

MATERIALS AND METHODS

Chemicals. L-[2,3,4,5-^{3}H]Arginine was purchased from Amersham Corp. (specific activity, 77 Ci/mmol). (6*R*)-5,6,7,8-Tetrahydro-L-biopterin (BH_4) was obtained from Research Biochemical International. L-Arginine, L-histidine,

† This work was supported by U.S. Public Health Service Grants GM44911, GM21337, and Welch C336.

* To whom correspondence should be addressed at the Division of Hematology, Department of Internal Medicine, University of Texas Medical School at Houston, P.O. Box 20708, Houston, TX 77225.

‡ University of Texas Medical School at Houston.

§ Rice University.

[1] Abbreviations: NO, nitric oxide; NOS, nitric oxide synthase; eNOS, endothelial nitric oxide synthase; nNOS, neuronal nitric oxide synthase; MCD, magnetic circular dichroism; EPR, electron paramagnetic resonance; BH_4, (6*R*)-5,6,7,8-tetrahydro-L-biopterin; 2′&3′-AMP, adenosine 2′- and 3′-monophosphate; CHAPS, 3-[(3-cholamidopropyl)-dimethylammonio]-1-propanesulfonate; Sf9 cells, *Spodoptera frugiperda* cells.

S0006-2960(98)00133-0 CCC: $15.00
Published on Web 04/09/1998

Table 1: Soret Optical and MCD Parameters of eNOS and Its Complex with Different Imidazole Derivatives

complex	spin state	K_d (mM)	λ_{max} (nm)	ϵ_{max} (mM^{-1} cm^{-1})	$\Delta\epsilon_{max-min}$ (mM^{-1} cm^{-1})	$\Delta\epsilon_{max-min}$ (M tesla cm)$^{-1}$
eNOS	LS/HS		398	108	−	24
imidazole[a]	LS	0.15	428	112	80	110
1-phenylimidazole	LS	>200	ND	ND	ND	ND
1-(4-hydroxyphenyl)imidazole	LS	0.24	427	112	62	84
1-(3-aminopropyl)imidazole	LS	0.57	427	124	67	94
1-benzylimidazole	LS	0.35	427	109	73	90
1-butylimidazole	LS	0.52	427	104	74	96
2-methylimidazole[a]	LS	17.5	427	98	42	60
2-propylimidazole	LS/HS	2.7	427	104	41	74
2-isopropylimidazole	LS/HS	1.96	426	116	54	84
2-phenylimidazole	HS/LS	1.4	396	∼100	11	24
2-aminoimidazole	HS	0.8	394	112	11.5	32
4-methylimidazole[a]	LS	0.87	426	∼104	48	79
4-phenylimidazole	HS	0.87	396	∼104	11	28
L-histidine[a]	HS	1.7	396	108	12.5	35
histamine	LS	65	422	ND	52	ND

[a] Data from ref *16*.

histamine, NADPH, adenosine 2′- and 3′-monophosphate (2′- and 3′-AMP), CHAPS, calmodulin, and all chemicals used for purification were purchased from Sigma. Imidazole, 1-butylimidazole, 1-benzylimidazole, 1-(3-aminopropyl)-imidazole, 1-(4-hydroxylphenyl)imidazole, 1-phenylimidazole, 2-aminoimidazole, 2-methylimidazole, 2-propylimidazole, 2-isopropylimidazole, 2-phenylimidazole, 4-methylimidazole, and 4-phenylimidazole and other chemicals used as ligands are Aldrich products.

Protein Expression, eNOS Purification, and NOS Activity Assay. Recombinant human endothelial nitric oxide synthase (eNOS) was prepared using the baculovirus expression system used in our laboratory. Expression and purification of recombinant proteins were essentially the same as described previously (*7*, *15*). NOS activity was assayed by measuring the conversion of tritium-labeled L-arginine to L-citrulline according to the published procedures (*13*). A 3-min incubation of the reaction mixture at 37 °C before quenching was used to maintain a linear production of L-citrulline.

Optical Absorption, MCD, and EPR Spectroscopy. Optical spectra were recorded in a Hewlett-Packard diode array spectrophotometer (Model 8452 or 8453). Magnetic circular dichroism (MCD) spectra were obtained using a Jasco J-500C spectrometer with a 1.3 T electromagnet calibrated with camphorsulfonic acid and potassium ferricyanide (*31*). All optical and MCD measurements were performed at room temperature (24 °C). EPR was recorded at liquid helium temperature on a Varian E-6 spectrometer with an Air Product liquid helium transfer line (*16*). A Hewlett-Packard frequency counter was used to monitor the microwave frequency. EPR parameters including g values, V, and Δ, the rhombic and axial ligand field terms for low-spin heme complexes, and the ratio of rhombic (E) and axial (D) ligand field components for high-spin heme complexes were determined as previously described (*16*).

Determination of Ligand Binding Affinity. The binding isotherm and dissociation constant for each ligand were obtained by an optical titration procedure as previously described (*7*).

Pyridine Hemochromogen Assay. Heme content was determined by the formation of pyridine hemochromogen (*17*). Briefly, the spectrum of isolated eNOS containing 0.15 M NaOH, 1.8 M pyridine, and ∼100 μg of eNOS was first recorded, and the sample was then reduced by addition of a few grains of dithionite. The total heme content was quantitated from the difference spectrum (reduced minus oxidized bispyridine heme) using $\Delta A = 24$ mM^{-1} cm^{-1} at 556−538 nm.

Protein Determination. Protein was determined by BCA (*18*), modified Lowry (*19*), and quantification of tryptophan by magnetic circular dichroism (MCD) using L-tryptophan as standard ($A_{282} = 5500$ M^{-1} cm^{-1}) (*20*).

RESULTS

Heme Extinction Coefficient. The spectrum of the pyridine hemochromogen of eNOS displays absorbance peaks at 418, 524, and 556 nm with a 1:2 ratio of the absorbance at 524 and 556 nm, similar to the heme present in nNOS and iNOS (*30*). The millimolar absorbance at 398 nm of the resting eNOS was determined to be 135 mM^{-1} cm^{-1}. The heme stoichiometry was determined to be 0.5−0.6 mol of heme/mol of protein using three different methods for quantitation of protein concentration. The BCA and Lowry methods yielded very similar results to the noninvasive MCD quantitation of tryptophan residues in the protein sample assuming 22 tryptophans as deduced from the primary sequence. The heme millimolar absorbance we determined for the heme present in eNOS is somewhat higher than the published value for nNOS and iNOS (71−100 mM^{-1} cm^{-1}) (*32*, *22*). Very recent parallel measurements of heme and protein content of all three isoforms of NOS, including five eNOS samples, three nNOS samples, and one iNOS sample requested from different laboratories, and standard P450 proteins indicate that all P450 proteins we evaluated show ∼20% lower heme content in comparison with *b*- or *c*-type heme proteins under our experimental conditions. The correct value of the heme extinction of our eNOS sample should be in the vicinity of 100−110 mM^{-1} cm^{-1} (unpublished data), which is close to the value reported by Sono et al. (*22*).

Optical and MCD Characteristics. Imidazole and all 1-substituted imidazoles cause a type II spectral change (Table 1), and with the exception of 1-phenylimidazole, these analogues exhibited an affinity for eNOS around 1 mM as quantitated by optical titration (*7*). 1-(3-Aminopropyl)-imidazole shifted the eNOS Soret peak from 398 to 426 nm

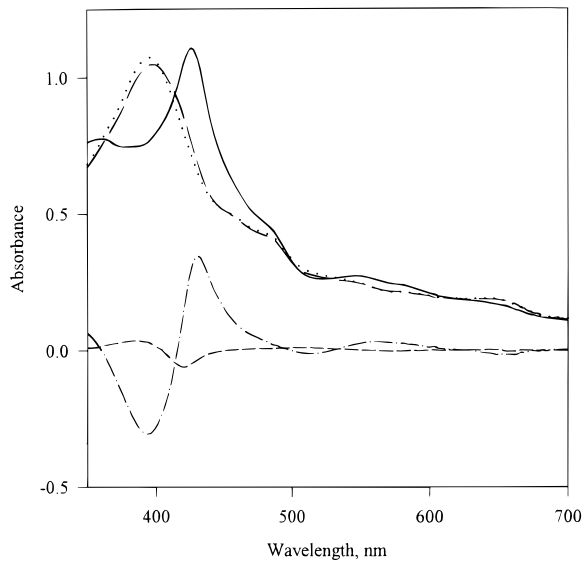

FIGURE 1: Spectral perturbation of eNOS heme caused by different imidazole derivatives. Optical spectra were obtained from 10.3 μM eNOS (dashed line), and from 10.3 μM eNOS plus either 15 mM 2-aminoimidazole (dotted line) or 10 mM 1-(3-aminopropyl)-imidazole (solid line) in 50 mM Tris buffer, pH 7.5−7.8, with 5 mM CHAPS, 1 mM DTT, and 10% glycerol at 24 °C. The difference spectra between ligand-bound and free eNOS were also included for 2-aminoimidazole (dashed line) and 1-(3-aminopropyl)-imidazole (dash, dot).

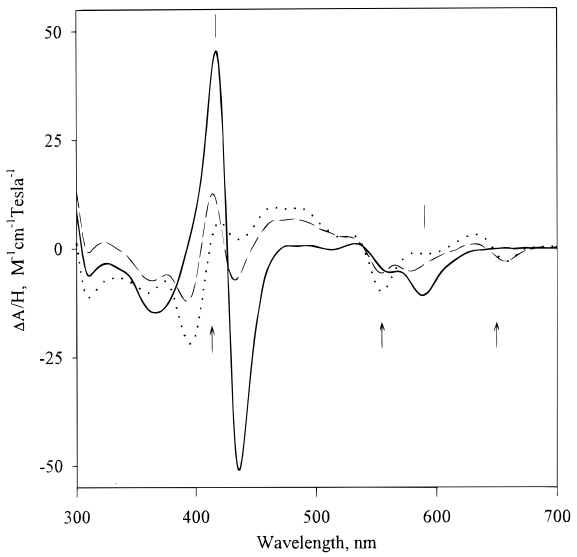

FIGURE 2: MCD spectra of resting eNOS (dashed line), 2-aminoimidazole (dotted line), and the 1-(3-aminopropyl)imidazole (solid line) complexes of eNOS. The sample conditions were the same as those described in Figure 1. The vertical lines identify the marker bands for low-spin heme, and arrows are the markers for high-spin heme.

with an increase in the millimolar absorption to 124 mM^{-1} cm^{-1}. The difference spectrum (eNOS imidazole complex *minus* eNOS) exhibits a peak at 432 nm and a trough at 394 nm. These spectral changes are very similar to those observed with imidazole and are typical of low-spin heme complex formation. In contrast, 2-aminoimidazole, which binds eNOS with a similar affinity as 1-(3-aminopropyl)-imidazole (K_ds of 0.8 and 0.57 mM, respectively), generated a type I spectral perturbation of eNOS with a 4-nm blue shift of the Soret peak and a difference spectrum which is inverted (Figure 1 and Table 1). Such spectral changes are typical for the conversion of a low-spin to a high-spin heme complex. These opposite effects of the two imidazole analogues indicate that these ligands interact differently with the eNOS heme center.

A set of MCD spectra parallel to the optical data of Figure 1 is shown in Figure 2. The low-spin 1-(3-aminopropyl)-imidazole eNOS complex shows a prominent signal centered at 427 nm; an additional band at 588 nm is also a marker for this low-spin imidazole complex. In contrast, a much smaller Soret MCD was observed for the high-spin 2-aminoimidazole complex, and two different marker bands are present in the visible region at 555 and 656 nm. The MCD spectrum of the resting eNOS appears to have spectral features observed in both imidazole complexes, i.e., the 656 nm charge-transfer band and both the 555 and 588 nm minima, though with smaller signal amplitudes, implying that the eNOS heme is present as a mixture of high- and low-spin states. The amplitude of the Soret MCD of both resting eNOS and e-NOS treated with either L-arginine or imidazole was temperature dependent as is expected for a paramagnetic species; however, the signal amplitude deviated significantly from Curie behavior. The observed deviation is not consistent with a simple equilibrium between high-spin and low-spin heme (*31*), and its origin is being investigated.

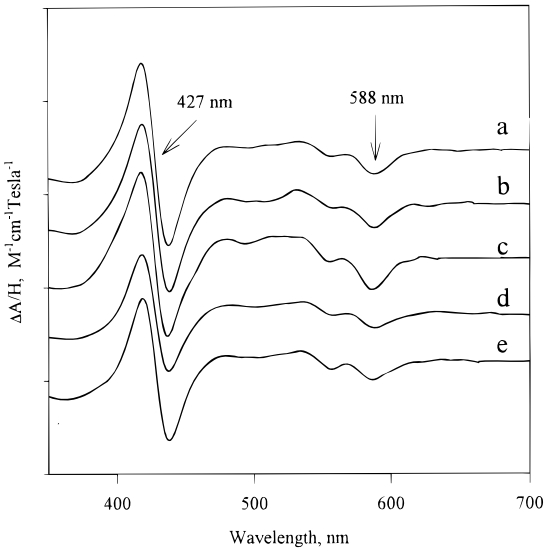

FIGURE 3: MCD spectra of low-spin imidazole derivatives of eNOS. The spectra of imidazole (a), 1-benzylimidazole (b), 1-butylimidazole (c), 2-propylimidazole (d), and 2-isopropylimidazole (e) complexes of eNOS were obtained in 50 mM Tris buffer, pH 7.5−7.8, with 5 mM CHAPS, 1 mM DTT, and 10% glycerol at 24 °C. The enzyme concentration used was 3−5 μM, and the ligand concentrations were 10 times the value of K_ds (Table 1). The spectra shown are representative of three sets of experiments.

eNOS complexes with 1-benzylimidazole and 1-butylimidazole exhibited MCD spectra extremely similar to that of imidazole both in line shape and in amplitude, indicating formation of practically pure low-spin heme complexes (Figure 3, spectra b, c, and Table 1). On the other hand, 2-propyl- and 2-isopropylimidazole, while giving MCD spectra similar in shape to that of imidazole had reduced amplitude (Figure 3, spectra d, e). Complexes formed by these latter two 2-substituted imidazoles apparently have their heme also present in the high-spin state, consistent with their lower absorption coefficient in the Soret (Table 1). Similar results were found with 2-methylimidazole (Table 1) which

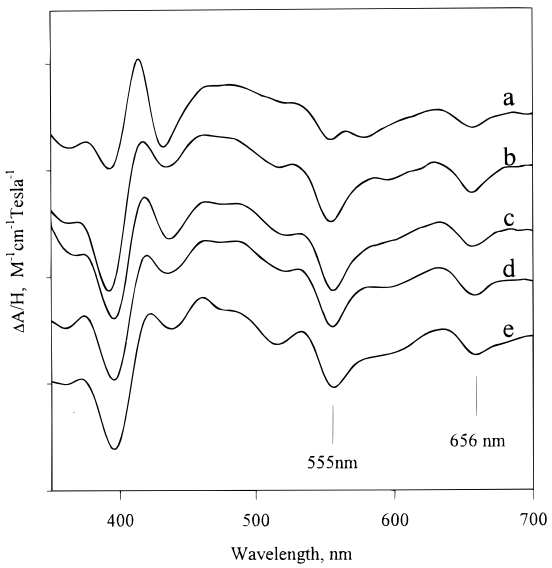

FIGURE 4: MCD spectra of high-spin imidazole derivatives of eNOS. MCD spectra were obtained for resting eNOS (a), eNOS plus L-arginine (b), eNOS plus L-histidine (c), eNOS plus 2-aminoimidazole (d), and eNOS plus 2-phenylimidazole (e). The experimental conditions were the same as those described in Figure 3.

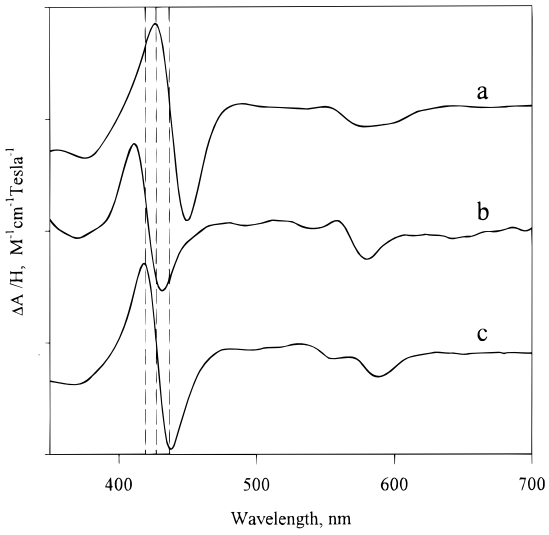

FIGURE 5: Low-spin MCD component in resting eNOS. Arithmetic subtraction of the MCD spectrum of the 2-aminoimidazole−eNOS complex (spectrum d in Figure 4, scaled to 60%) from that of resting eNOS gives the MCD spectrum for the low-spin component (b). MCD spectra of the low-spin C-based cyanide (a) and N-based imidazole (c) eNOS complexes are juxtaposed for comparison. Vertical dashed lines indicate the cross-over points of the Soret features.

yields a predominantly low-spin heme complex with eNOS though with a significant proportion present as the high-spin complex. The other 2-substituted imidazole, 2-phenylimidazole, produced essentially complete high-spin heme formation with eNOS, similar to that found with 2-aminoimidazole but differing from that observed with 2-methylimidazole (Table 1).

Imidazole analogues with substituents at the 4-position, like 2-substituted imidazoles, also yielded both low-spin and high-spin complexes with eNOS (Table 1). For example, histamine and 4-methylimidazole derivatives of eNOS are mainly low-spin, while 4-phenylimidazole and L-histidine led to an almost completely high-spin heme complex. Except for L-histamine, the other 4-substituted imidazoles all exhibit a K_d around 1 mM (Table 1). MCD spectra of the 2-aminoimidazole, L-histidine, and 2-phenylimidazole complexes display features at 555 and 656 nm troughs observed with the fully high-spin eNOS produced by L-arginine (Figure 4, c−e vs b). Comparison of the MCD spectra of resting eNOS and eNOS treated with L-arginine clearly indicates that the resting eNOS is composed of both low- and high-spin heme (Figure 4, spectra a and b). To obtain the MCD spectrum of the low-spin heme species present in resting eNOS, we subtracted different proportions of the spectrum of the fully high-spin spectrum (that of either the 2-aminoimidazole- or the L-arginine-treated sample) from that of the resting enzyme. The difference spectrum which show minimal high-spin heme signals at 555 and 656 nm was achieved by subtracting 60% of the spectrum of the pure high-spin eNOS complex from that of the resting enzyme (Figure 5, spectrum b). This difference spectrum exhibits the 588 nm marker band of the low-spin heme and a Soret crossover at 418 nm; this is distinct from that of the imidazole (427 nm, Figure 5c) or cyanide derivatives (438 nm, Figure 5a), implying that the distal heme ligand of low-spin eNOS is probably not a C- or N-based ligand.

EPR Analysis of Imidazole Derivatives. EPR of complexes formed between eNOS and 10 different imidazole analogues were recorded together with resting eNOS and L-arginine-treated eNOS (Figure 6). The EPR parameters and the corresponding rhombic and axial ligand-field components of both the high- and low-spin heme complexes are listed in Table 2. Ligands which generated mainly low-spin heme complexes are 1-butylimidazole, 1-benzylimidazole, 1-(3-aminopropyl)imidazole, 1-(4-hydroxyphenyl)imidazole, and 2-isopropylimidazole (Figure 6, a−e); ligands that produce mainly high-spin heme complexes include 2-aminoimidazole, 4-phenylimidazole, 2-phenylimidazole, and L-histidine (Figure 6, i−l). 2-Methylimidazole, 2-propylimidazole, and resting eNOS gave EPR spectra which were mixture of both high-spin and low-spin components (Figure 6, f−h).

The high-field region of each sample was rerun with slightly different instrument conditions to resolve details of the low-spin heme signals (Figure 7). The heme geometries of these low-spin complexes formed with different imidazole analogues are very similar. g_{mid} is centered in a very narrow region (2.29−2.30), g_{min} ranges from 1.8 to 1.84, and g_{max} varies from 2.56 to 2.61. In contrast, g_{min} and g_{max} of one of the resting eNOS low-spin heme centers are much closer to the g_{mid} than those of imidazole−heme complexes (1.90 and 2.42, respectively, and Table 2), implying that a different distal ligand is present in this low-spin eNOS.

Some low-spin imidazole analogues appear to induce more than one low-spin species as detected by EPR line broadening and band splitting at the positions of g_{min} and g_{max}. This finding is similar to our earlier observation for pH-dependent changes of EPR for eNOS complexes with imidazole and 4-methylimidazole (*16*). These pH-dependent changes were also observed for four other different low-spin complexes: 1-(3-aminopropyl)imidazole, 1-(4-hydroxyphenyl)imidazole, 2-isopropylimidazole, and 1-benzylimidazole (Figure 8). Acidification of these samples caused a shift of the heme to

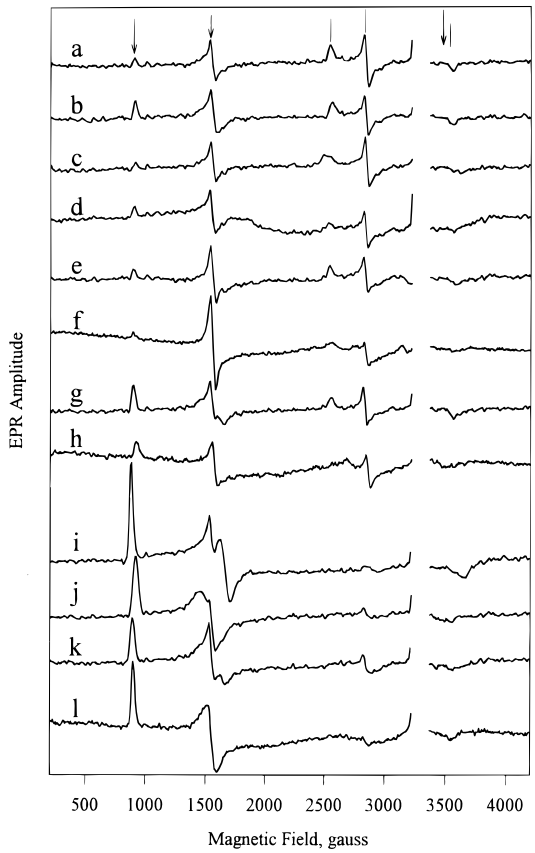

FIGURE 6: Effect of different imidazole homologues on the EPR spectrum of eNOS. Enzyme concentrations were 8−12 μM. The buffer and ligand concentrations were the same as those described in Figure 3. Ligands used for each spectrum are 1-butylimidazole (a), 1-benzylimidazole (b), 1-(3-aminopropyl)imidazole (c), 1-(4-hydroxyphenyl)imidazole (d), 2-isopropylimidazole (e), 2-methylimidazole (f), 2-propylimidazole (g), resting eNOS (h), 2-aminoimidazole (i), 4-phenylimidazole (j), 2-phenylimidazole (k), and L-arginine (l). EPR conditions were 10 mW microwave power, 10 G modulation, and 11 K. The g values and other parameters of each EPR sample are shown in Table 2. Arrows indicate the high-spin components, and vertical bars indicate the low-spin components.

Table 2: EPR Parameters of eNOS and Its Complex with Different Imidazole Derivatives

ligand	spin	g_x	g_y	g_z	% rhombicity	Δ (λ)	V (λ)
		1.84		2.54	49.0	4.80	2.73
eNOS	1/2		2.30				
		1.90		2.42	33.1	5.70	1.63
	5/2	7.67	4.34	1.84	20.8		
		1.75		2.70	61.9	4.00	2.50
imidazole	1/2		2.30				
		1.83		2.57	51.9	4.71	2.44
		1.83		2.53	44.4	4.71	2.09
1-(4-hydroxyphenyl)-imidazole	1/2		2.30				
		1.84		2.57	57.1	4.70	2.68
		1.80		2.61	56.2	4.44	2.50
1-(3-aminopropyl)-imidazole	1/2		2.29				
		1.82		2.54	47.6	4.66	2.22
1-benzylimidazole	1/2	1.83	2.30	2.57	50.6	4.66	2.36
1-butylimidazole	1/2	1.83	2.29	2.56	51.4	4.73	2.42
		1.82		2.56	49.3	4.61	2.27
2-methylimidazole	1/2		2.30				
		1.88		2.48	40.4	5.29	2.13
2-propylimidazole	1/2	1.84	2.30	2.56	49.8	4.76	2.34
	5/2	7.73	4.26	1.92	21.7		
		1.82		2.56	48.4	4.59	2.22
	1/2		2.30				
2-isopropylimidazole		1.83		2.54	46.0	4.69	2.16
	5/2	7.78	4.28	1.82	21.9		
2-phenylimidazole	5/2	7.79	4.20	1.85	22.4		
2-aminoimidazole	5/2	7.86	4.12	1.79	23.4		
		1.81		2.66	65.6	4.54	2.98
4-methylimidazole	1/2		2.28				
		1.83		2.57	55.1	4.77	2.63
4-phenylimidazole	5/2	7.46	4.42	1.86	19.0		
L-histidine [a]	5/2	7.71	4.19	1.81	22.0		

[a] Data from ref *16*.

a geometry of lower rhombicity, following the trend found earlier for imidazole and 4-methylimidazole (Figure 8 and Table 2).

A correlation analysis between heme rhombicity and the tetragonal field of these low-spin imidazole−heme complexes was performed according to the Blumberg−Peisach convention (*21*). The data clustered nicely in the *P* zone defined by a rhombicity between 0.47 and 0.63, and tetragonality between 4 and 5 (Figure 9). Compared to $P450_{cam}$ and chloroperoxidase and their complexes with different imidazole analogues, eNOS low-spin complexes overlap significantly with those of chloroperoxidase but not $P450_{cam}$. Some O-ligand and C-ligand derivatives of these three enzymes are also included in the diagram. For individual enzyme species, the positions of complexes with O-ligands overlap those with N-ligands but appear to be separate from those of C-ligand complexes. However, this distal ligand dependent localization on the Truth Diagram is not clear-cut using either the Blumberg−Peisach axis convention or that of Griffiths (data not shown). One of the low-spin heme centers in resting eNOS is located away from the cluster of imidazole complexes (Figure 9, +) and appears to indicate that the distal ligand is not nitrogen-based in this species.

EPR in the low-field region, 800−1000 G, was further examined for small variations in the high-spin heme EPR in eNOS. The most prominent perturbations are the low-field shift to $g = 7.86$ by 2-aminoimidazole and the high-field shift to $g = 7.46$ by 4-phenylimidazole (Figure 10 and Table 2). This 0.4 unit change in g_{max} of eNOS is the largest observed so far with ligands which yield high-spin complexes and type I spectral changes. The 2-substituted imidazoles including 2-phenyl, 2-methyl, 2-propyl, and 2-isopropyl induced a low-field shift of g_{max}, but the extent is much less than that found with 2-aminoimidazole (Figure 10 and Table 2).

The high-spin signals found in resting enzyme and in four 1-substituted imidazole analogues aligned exactly at $g = 7.67$, indicating that the high-spin heme species found in the 1-substituted imidazole complexes are the same as that present in resting eNOS. The amplitude of g_{max} of the high-spin heme appears to be proportional to the percentage of the high-spin heme component in the sample, with 2-aminoimidazole- or L-arginine-treated eNOS containing almost exclusively high-spin heme. With very similar line widths at g_{max}, we used the amplitude of this signal to estimate the amount of high-spin species, using 2-aminoimidazole as the standard for 100% high-spin.

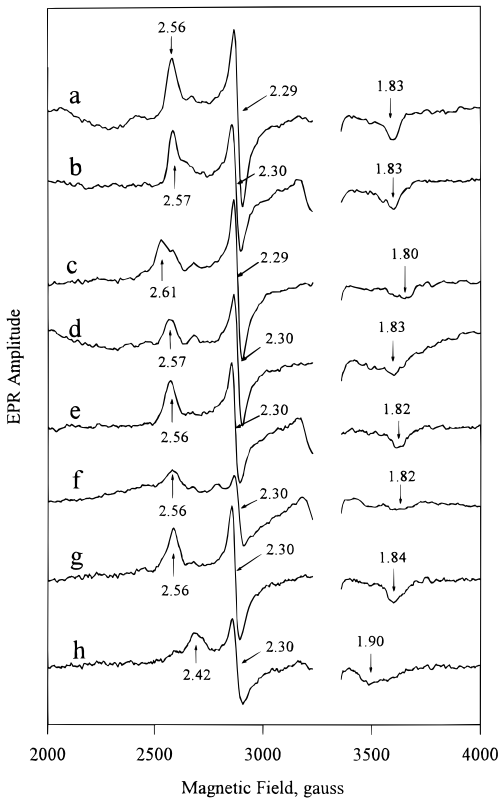

FIGURE 7: EPR of different low-spin heme imidazole complexes of eNOS. Enzyme and ligand concentrations are the same as those described in Figure 6. Ligands used were 1-butylimidazole (a), 1-benzylimidazole (b), 1-(3-aminopropyl)imidazole (c), 1-(4-hydroxyphenyl)imidazole (d), 2-isopropylimidazole (e), 2-methylimidazole (f), 2-propylimidazole (g), and resting eNOS (h). Spectra were recorded at 4 mW power, 20 G modulation, and 11 K. The radical region of each spectrum was cropped for clarity. Numbers next to each arrow are the *g* values.

Heme in Different Spin States. Estimates of the proportion of high- and low-spin heme in each of the ligand complexes were conducted on the UV−vis, MCD, and EPR spectral data sets. In the case of the optical and MCD data, the molar absorption of the Soret peak for the cyanide derivative was set as the standard of 100% low-spin. Correlation of the estimated low-spin heme population in each heme complex was done both between UV−vis and MCD and between MCD and EPR as shown in Figure 11. In both cases, an approximately unit slope correlation was observed for eNOS complexes formed with nine different imidazole analogues.

DISCUSSION

We evaluated the influence of a series of imidazole derivatives having substituent at the 1-, 2-, and 4-positions of imidazole on the heme structure changes of eNOS. The imidazole analogues studied generated low-spin (type II spectral change), high-spin (type I spectral change), and mixed-spin eNOS heme complexes (Tables 1 and 2). The contrasting spectral perturbation of eNOS heme induced by different imidazole analogues gave additional examples to our previous reports for the contrasting spectral perturbation of eNOS heme by pyridine, pyrimidine, and thiazole and their homologues (*7*, *16*). Thus, low-spin heme complexes are formed by direct ligation of the imidazole moiety to the heme iron while the high-spin complexes are formed by

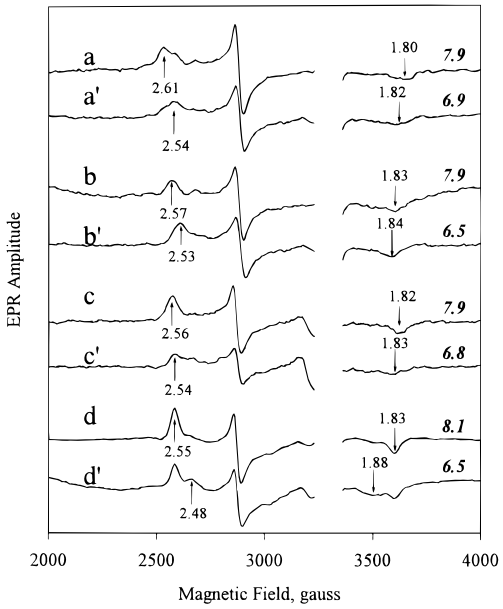

FIGURE 8: Effect of pH on the low-spin EPR of imidazole derivatives. EPR spectra of 1-(3-aminopropyl)imidazole (a, a′), 1-(4-hydroxyphenyl)imidazole (b, b′), 2-isopropylimidazole (c, c′), and 1-benzylimidazole (d, d′) were recorded first at higher pH, and then the same samples were recorded at lower pH. Actual pH is shown inside the figure. The other experimental conditions were the same as in Figure 6.

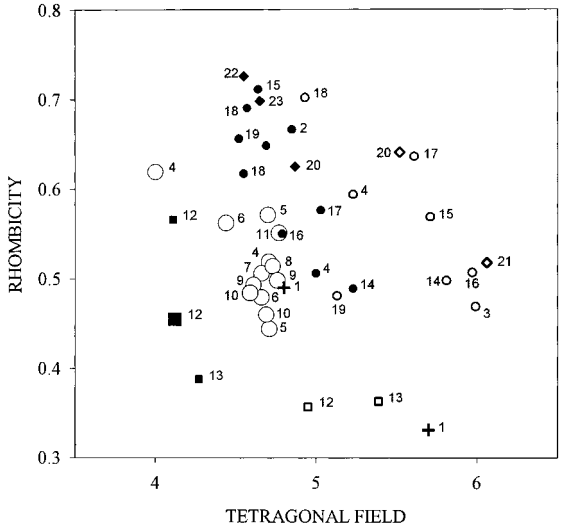

FIGURE 9: Complexes of eNOS (large symbols), choloroperoxidase (small closed symbols), and P450 (small open symbols) with N-ligands (circles), C-ligands (squares), and O-ligands (diamonds) were analyzed by the technique of Blumberg and Peisach (*21*) and presented as a "Truth Diagram". For clarity, only the *P*-zone is displayed. The two low-spin forms of resting eNOS are also included (crosses). The ligands are as follows: (1) resting eNOS; (2) resting chloroperoxidase; (3) resting $P450_{cam}$; (4) imidazole; (5) 1-(4-hydroxyphenyl)imidazole; (6) 1-(3-aminopropyl)imidazole; (7) benzylimidazole; (8) butylimidazole; (9) 2-methylimidazole; (10) 2-isopropylimidazole; (11) 4-methylimidazole; (12) cyanide; (13) *N*-butylisocyanide; (14) 1-phenylimidazole; (15) 4-phenylimidazole; (16) pyridine; (17) azide; (18) thiocyanate; (19) selenocyanate; (20) formate; (21) acetate; (22) methanol; (23) ethanol.

ligand binding at a site adjacent to the heme, causing the expulsion of the original distal ligand.

In this study, three spectroscopic methods have been applied to evaluate the effect of imidazole analogues on heme spin states and geometry. Data obtained by these three

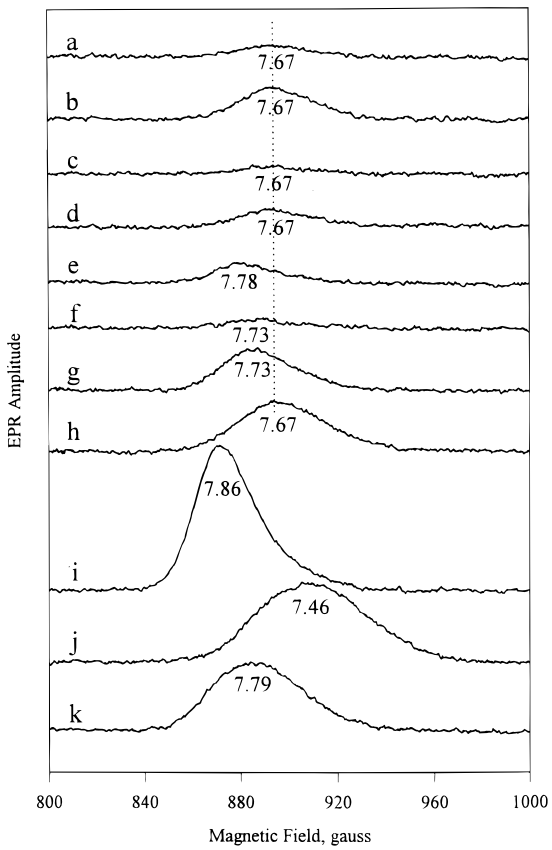

FIGURE 10: Shift of the low-field high-spin heme EPR signal by imidazole derivatives. The spectra follow the same sequence as shown in Figure 6. Numbers are the g_{max} values. The other conditions are the same as in Figure 6. The vertical dash locates $g = 7.67$.

methods agree quite nicely with one another, even though the EPR data were acquired at liquid helium temperature. This correlation of spin-state distribution measured by low-temperature EPR and room-temperature optical and MCD spectroscopy implies that there is no drastic temperature dependence of heme spin state. MCD and EPR are superior to UV−vis in quantitation of the spin states because the flavin background interferes in the latter.

Because the EPR parameters are very similar, MCD is the best in assigning the distal ligand. The MCD spectra of resting eNOS and L-arginine-treated eNOS resemble closely those reported for nNOS and those of 5-coordinate $P450_{cam}$ and chloroperoxidase (*22*). The difference spectrum obtained by subtracting the high-spin contribution of resting eNOS (Figure 5) shows a Soret crossover at 418 nm which is clearly different from that of imidazole (N-ligand) and cyanide (C-ligand) derivatives. The similarity of this difference spectrum with those of MCD spectra recorded for $P450_{cam}$ and chloroperoxidase containing a sixth O-ligand (*23*) provides a strong indication that the low-spin heme species of resting eNOS has an O-ligand, such as water. MCD, on the other hand, is rather insensitive to changes in heme geometry. None of the spin-state markers found in the MCD spectra (Figures 2−4) provide any information about heme geometry.

EPR is superior in revealing subtle changes in heme geometry and is particularly useful in differentiating the different structural perturbations of the 5-coordinate heme complexes (Figure 10). We have found four types of high-spin heme complexes generated by different imidazole

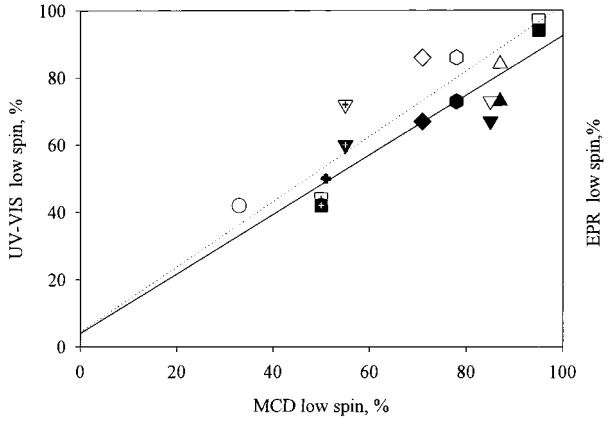

FIGURE 11: Correlation of heme spin-state distribution between Soret optical and MCD (open symbols), and between MCD and EPR (solid symbols) intensity of eNOS complexes formed with imidazole homologues. For UV−vis and MCD, the signal intensity of the cyanide−eNOS complex was taken as 100% low-spin. Quantitation of the high-spin heme percentage from EPR data was standardized against the low-field rhombic signal of L-arginine-treated eNOS (100% high spin). The ligands used were imidazole (□, ■), 1-butylimidazole (△, ▲), 1-benzylimidazole (▽, ▼), 1-(3-aminopropyl)imidazole (⬡, ⬢), 1-(4-hydroxylphenyl)imidazole (◇, ◆), 2-isopropylimidazole (downward triangles with inscribed plus signs), 4-methylimidazole (+), 2-methylimidazole (○), 2-propylimidazole (squares with inscribed plus signs).

homologues as judged by their EPR spectra: The first type is the unreacted resting eNOS which shows $g_{max} = 7.67$, identical to that of the resting eNOS and L-arginine-treated eNOS (Figures 6 and 10).

The second type of high-spin heme results from direct steric strain on porphyrin by the substituent at the 2-position of imidazole, leading to a slight increase of rhombicity (g_{xmax} at 7.73−7.79 region). A similar example has been reported for the 2-phenylimidazole complex of $P450_{cam}$, for which crystallographic data are available (*24*); these crystal data reveal that 2-phenylimidazole adopts an inverted orientation with the imidazole ring pointing away from the heme iron and the phenyl group pointing toward heme iron and within 5 Å. There is also a rearrangement of the distal pocket so that a few polar amino acid residues become more exposed to the imidazole moiety and participate in formation of two hydrogen bonds, while in the structure of 1-phenylimidazole $P450_{cam}$ all amino acids surrounding the ligand are hydrophobic in nature (*24*). A similar ligand orientation and protein structural perturbation might occur upon association of the 2-substituted imidazoles with eNOS. In contrast to the case with eNOS, X-ray and EPR data of the complex formed between $P450_{cam}$ and 2-phenylimidazole reveal a 6-coordinate low-spin heme complex (*24*, *25*) that is not due to a direct ligation of the imidazole to the heme iron but represents the presence of an axial water ligand.

The third type of high-spin complex is generated by a bulky group at position 4 of imidazole. This is shown by a comparison of the EPR of 4-methylimidazole and either 4-phenylimidazole or L-histidine. Increasing the size of the substituent caused a shift in composition from low- to high-spin heme. It is not clear though why 4-phenylimidazole led to a decrease of rhombicity ($g_{min} = 7.46$) while L-histidine caused an increase of rhombicity of the heme ($g_{max} = 7.71$).

The fourth type is unique for 2-aminoimidazole which generated the most rhombic eNOS EPR spectrum with the

shift of g_{max} being much bigger than with other 2-substituted imidazoles (g_{max} = 7.86). 2-Aminoimidazole has three nitrogen groups which could generate a low-spin eNOS complex, yet it yielded a high-spin complex. Simple steric strain on the porphyrin plane cannot be the whole story because the 2-amino group is not as bulky as the 2-phenyl group. On the other hand, a methyl group, which is equivalent in size to an amino group, at the 2-position of imidazole led to the formation of a low-spin eNOS complex. These results are most simply interpreted as a direct binding of 2-aminoimidazole to the guanidine subdomain of L-arginine, resulting in a heme structural change.

The high sensitivity of EPR in revealing the subtle changes in geometry in the 5-coordinate nNOS has also been demonstrated recently by Salerno and co-workers using different substrate analogues (*26*, *27*). The changes in ligand from *N*-nitroarginine to thiocitrulline caused a 0.5 unit shift of g_{max} (from 7.26 to 7.76) and a corresponding change in the *E*/*D* ratio from 0.059 to 0.087. Thus, the EPR of the 5-coordinate heme of NOS can be a very effective sensor for changes which occur both in the substrate binding pocket as well as in the heme distal ligand pocket.

With the exception of 1-phenylimidazole which has a very poor affinity for eNOS ($K_D \gg 100$ mM), all 1-substituted imidazoles used in our study yield a low-spin heme complex. This is hard to rationalize as both 1-(4-hydroxyphenyl)-imidazole and 1-benzylimidazole showed a K_d of less than 1 mM. About a 20-fold difference in the potency of 1-phenylimidazole in inhibiting human iNOS and eNOS activity (IC_{50} of 33 and 611 mM, respectively) has also been observed (*14*). This result points to a structural difference of the heme distal pocket between these isoforms.

Both low-spin and high-spin heme complexes were induced by 2- and 4-substituted imidazoles, and the transition from low-spin to high-spin appears to be a function of the size of the substituent. Thus, 2-methylimidazole yielded low-spin eNOS and 2-phenylimidazole gave high-spin eNOS while 2-propyl- and 2-isopropylimidazole caused a mixture of high- and low-spin eNOS. A similar trend was found for the 4-substituted imidazoles. However, this similarity in the size-dependent transition of heme spin state between 2- and 4-substituted imidazoles originates from different mechanisms. The spin transition for 2-substituted imidazoles is a consequence of direct steric strain of the substituent with the heme plane, whereas the height of the distal heme pocket provides the steric strain for the 4-substituted imidazoles. This ceiling height for eNOS was estimated to be 6.7 to ~7 Å gauged by serial rigid planar ligands (*7*) and by formation of *N*-aryl protoporphyrin from serial arylazenes (*28*).

Low-spin eNOS complexes all show similar *g* anisotropy and are clustered in a very focused area in the Truth Diagram (Figure 9) with the single low-spin complex formed by imidazole as the only outlier. This close proximity of various imidazole eNOS complexes on the Truth Diagram seems to validate its use in identifying the distal heme ligand. Comparing those low-spin heme complexes for eNOS, chloroperoxidase, and $P450_{cam}$ with N-, O-, or C-ligand at the sixth position, C-ligand complexes are clearly separated from complexes with N- or O-ligand. However, there is no clear separation between complexes with O- or N-ligand for either protein, thus limiting the usage of Truth Diagram analysis in ligand assignment. This limitation was again a consequence of the leveling effect of the strong proximal thiolate ligand as previously reported (*29*).

There are two different low-spin species in resting eNOS identified by EPR (*16*). On the Truth Diagram, these two low-spin hemes are located in quite different regions. The first is localized in the cluster of imidazole complexes while the second is located at the lower margin of the *P* zone (Figure 9). MCD data suggested that the low-spin heme has an O-ligand at the sixth position. Whether these two low-spin forms of eNOS distinguished by EPR represent hemes with two different O-ligands or the same O-ligand but differing heme geometry is unclear. Two low-spin species have also been observed for the complexes formed between eNOS and both imidazole and 4-methylimidazole (*16*), and a similar pH dependence of the mutual interconversion between the low-spin heme species was observed for all the imidazole homologues used in this work (Figure 8). Whether this result indicates that the two heme sites in the functional dimer have a different geometry or simply that there are two types of heme randomly distributed in the eNOS sample is unclear. This subtle difference in heme geometry of NOS, however, is not easily revealed by optical binding studies between CO, cyanide, imidazole, or L-arginine ligands and its ferric heme (*6*, *7*, *12*), or EPR binding study between NO and its ferrous heme (*33*).

REFERENCES

1. Kerwin, J. F., Jr., Lancaster, J. R., Jr., and Feldman, P. L. (1995) *J. Med. Chem. 38*, 4343−4358.
2. Feldman, P. L., Griffith, O. W., and Stuehr, D. J. (1993) *Chem. Eng. News 71*, 26−38.
3. Masters, B. S. S., McMillan, K., Sheta, E. A., Nishimura, J. S., Roman, L. J., and Martasek, P. (1996) *FASEB J. 298*, 249−258.
4. Knowles, R. G., and Moncada, S. (1994) *Biochem. J. 298*, 249−258.
5. White, K. A., and Marletta, M. A. (1992) *Biochemistry 31*, 6627−6630.
6. Matsuoka, A., Stuehr, D. J., Olson, J. S., Clark, P., and Ikeda-Saito, M. (1994) *J. Biol. Chem. 269*, 20335−20339.
7. Berka, V., Chen, P.-F., and Tsai, A.-L. (1996) *J. Biol. Chem. 271*, 33293−33300.
8. Mayer, B., Klatt, P., Werner, E. R., and Schmidt, K. (1994) *FEBS Lett. 350*, 199−202.
9. Wolff, D. J., Datto, G. A., Samatovicz, R. A., and Tempsick, R. A. (1993) *J. Biol. Chem. 268*, 9425−9429.
10. Wolff, D. J., Lubesk'e, A., and Umansky, S. (1994) *Arch. Biochem. Biophys. 314*, 360−366.
11. McMillan, K., and Masters, B. S. S. (1993) *Biochemistry 32*, 9875−9880.
12. Roman, L. J., Sheta, E. A., Martasek, P., Gross, S. S., Liu, Q., and Masters, B. S. S. (1995) *Proc. Natl. Acad. Sci. U.S.A. 92*, 8428−8432.
13. Chen, P.-F., Tsai, A.-L., and Wu, K. K. (1994) *J. Biol. Chem. 269*, 25062−25066.
14. Chabin, R. M., McCauley, E., Calaycay, J. R., Kelly, T. M., MacNaul, K. L., Wolfe, G. C., Hutchinson, N. I., Madhusudan-araju, S., Schmidt, J. A., Kozarich, J. W., and Wong, K. K. (1996) *Biochemistry 35*, 9567−9575.
15. Chen, P.-F., Tsai, A.-L., Berka, V., and Wu, K. K. (1996) *J. Biol. Chem. 271*, 14631−14635.
16. Tsai, A.-L., Berka, V., Chen, P.-F., and Palmer, G. (1996) *J. Biol. Chem. 271*, 32563−32571.
17. Hauger, D. A., and Coon, M. J. (1976) *J. Biol. Chem. 151*, 7929−7939.
18. Smith, P. K., Krohn, R. I., Hermanson, G. T., Mallia, A. K., Gartner, F. H., Provenzano, M. D., Fujimoto, E. K., Goeke, N. M., Olson, B. J., and Klenk, D. C. (1985) *Anal. Biochem. 150*, 76−85.

19. Peterson, G. L. (1977) *Anal. Biochem. 83*, 346−356.
20. Holmquist, B., and Valee, B. L. (1973) *Biochemistry 12*, 4409−4417.
21. Blumberg, W. E., and Peisach, J. (1971) in *Probes and Structure and Function of Macromolecules and Membranes* (Chance, B., Yonetani, T., and Mildvan, A. S., Eds.) Vol. 2, pp 215−229, Academic Press, New York.
22. Sono, M., Stuehr, D. J., Ikeda-Saito, M., and Dawson, J. H. (1995) *J. Biol. Chem. 270*, 19943−19948.
23. Dawson, J. H., Andersson, L. A., and Sono, M. (1982) *J. Biol. Chem. 257*, 3606−3617.
24. Poulos, T. L., and Howard, A. J. (1987) *Biochemistry 26*, 8165−8174.
25. Lipscomb, J. D. (1980) *Biochemistry 19*, 3590−3599.
26. Salerno, J. C., McMillan, K., and Masters, B. S. S. (1996) *Biochemistry 35*, 11839−11845.
27. Salerno, J. C., Martasek, P., Roman, L. J., and Masters, B. S. S. (1996) *Biochemistry 35*, 7626−7630.
28. Gerber, N. C., Rodriguez-Crespo, I., Nishida, C. R., and Ortiz de Montellano, P. R. (1997) *J. Biol. Chem. 272*, 6285−6290.
29. Sono, M., and Dawson, J. H. (1982) *J. Biol. Chem. 257*, 5496−5502.
30. Stuehr, D. J., and Ikeda-Saito, M. (1992) *J. Biol. Chem. 267*, 20547−20550.
31. Vickery, L. E. (1978) *Methods Enzymol. 65*, 284−302.
32. Suehr, D. J., and Ikeda-Saito, M. (1992) *J. Biol. Chem. 267*, 20547−20550.
33. Migita, C. T., Salerno, J. C., Masters, B. S. S., Martasek, P., McMilan, K., and Ikeda-Saito, M. (1997) *Biochemistry 36*, 10987−10992.

BI980133L